Journal of Solid State Chemistry 182 (2009) 555–559

Contents lists available at ScienceDirect

Journal of Solid State Chemistry

journal homepage: www.elsevier.com/locate/jssc

Charge density measurement and bonding character in $LiNiO_2$

Jiefeng Cao [a], Chao Guo [a], Huamin Zou [a,b,*]

[a] Department of Physics, Wuhan University, Wuhan 430072, China
[b] Centre for Electron Microscopy, Wuhan University, Wuhan 430072, China

ARTICLE INFO

Article history:
Received 1 July 2008
Received in revised form
13 November 2008
Accepted 24 November 2008
Available online 3 December 2008

Keywords:
$LiNiO_2$
QCBED
Multipole refinement
Bond critical point
3*d* orbital population

ABSTRACT

Accurate low-order structure factors of $LiNiO_2$ were measured by quantitative convergent-beam electron diffraction (QCBED), and then transformed into X-ray structure factors with Mott formula. Combining the structure factors measured by electron diffraction with the structure factors from X-ray diffraction measurements, accurate charge density maps based on a multipole model were obtained. The parameters of the bond critical points (BCP) were calculated for topological analyses. It shows that closed-shell interactions exist between Ni and O atoms, and that the Ni–O and Ni–Ni bonds exhibit some covalent character. The calculated *d*-orbital occupancies show the charge deficiency at $e_g(e_g)$ orbital and charge surplus at $e_g(t_{2g})$ orbital. The remaining 29.12% population of $e_g(e_g)$ is also an indication of covalent component in the Ni–O bond. The unusual small κ_{defv} value of the O atom is also discussed.

1. Introduction

Lithium nickel oxide is one of the most widely used positive electrode materials for rechargeable lithium-ion batteries. The ideal transition-metal oxide $LiNiO_2$ belongs to space group $R\bar{3}m$, and is constructed by stacking NiO_2 layers and Li layers alternately (see Fig. 1). The electrochemical and magnetic properties of $LiNiO_2$ have been extensively studied by means of various experiments [1–6]. However, the charge density and orbital information have been studied only by theoretical calculations [7–9], and no experimental results about those have been reported so far.

The accuracy of the low-order crystal structure factors becomes crucial because the relatively weak bonding electrons mainly contribute to the reflections at low scattering angles. In measuring low-order structure factors, quantitative convergent-beam electron diffraction (QCBED) has the advantage over other methods due to the following reasons: By using QCBED technique, the dynamical interactions between low-angle reflections are taken into account accurately and can provide the extinction-free measurement of low-order structure factors. Second, in the QCBED technique, the convergent beam electron diffraction pattern can be taken from a perfect region of a crystal, the influence of scattering from defects is eliminated. QCBED has been proved to be very successful in measuring the electron density distribution of Cu_2O, MgO, $SrTiO_3$, etc. [10–12]. When the final set of structure factors is determined, the multipole refinement is carried out by using the XD program package [13] which is the program for least squares fitting of a multipole model to the experimental data. The *d*-orbital occupancies of transition-metal atoms can be derived from multipole population coefficients by using point-group-specific relations. And the associated topological properties at the bond critical points (BCP) can be obtained from the refinement of the experimental data, which are very useful to analyze the bond information.

In the present paper, eight low-order structure factors of $LiNiO_2$ are measured by using QCBED technique. By combining these measurements with single-crystal X-ray diffraction data, and using multipole refinement, accurate parameters of multipole model are obtained. From these results, the elaborate charge distributions are plotted, BCP in the Ni–O and Ni–Ni bonds are obtained, the role of 3*d* electrons of Ni atoms are also discussed.

2. Experiment

Polycrystalline samples of $LiNiO_2$ were prepared by the standard solid-state reaction method. Appropriate molar ratios of LiOH and $Ni(OH)_2$ powders with the purities higher than 99.9% were ground and blended in an agate mortar, and then heated at 600°C for 1 h in air. The reacted samples were then pulverized, pressed into pellets and sintered for 48 h at 720°C in an oxygen gas flow in a tubular furnace.

Powder X-ray diffraction experiments were carried out on the Bruker AXS D8-Advance diffractometer. The X-ray diffraction spectrum as shown in Fig. 2 indicates that the synthesized sample is $LiNiO_2$, and that there are no other impurity phases. The crystal

* Corresponding author at: Department of Physics, Wuhan University, Wuhan 430072, China. Fax: +86 27 68752569.
E-mail addresses: cjf_lazio@tom.com (J. Cao), hmzou@whu.edu.cn (H. Zou).

0022-4596/$ - see front matter © 2008 Elsevier Inc. All rights reserved.
doi:10.1016/j.jssc.2008.11.027

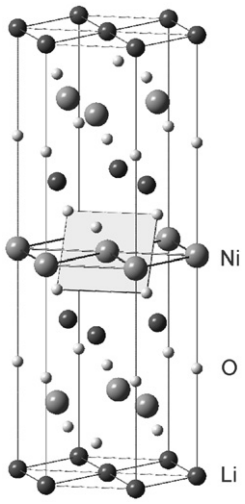

Fig. 1. Ideal crystal structure of $LiNiO_2$. The Li, Ni and O atoms occupy the 3*a*, 3*b* and 6*c* sites respectively. The plane, on which the charge density is plotted in Fig. 3, is shadowed in this figure.

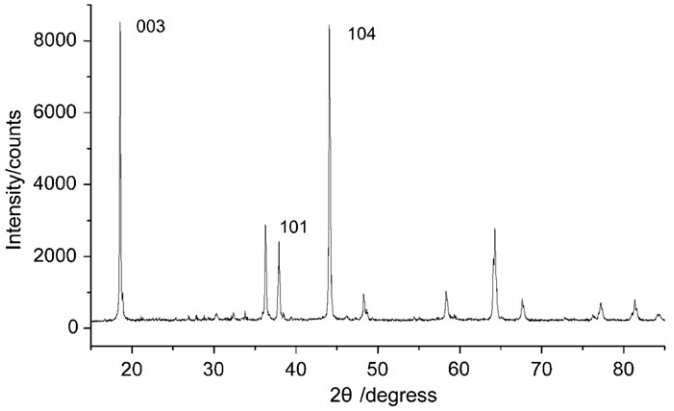

Fig. 2. X-ray diffraction pattern of $LiNiO_2$.

Table 1
Structure refinement models and their *R* values.

Model	Refined cation distribution	R_p	R_{wp}	χ^2
1	$(Li_{0.777}Ni_{0.223})_{3a}[Li_{0.223}Ni_{0.777}]_{3b}O_2$	7.387	10.244	3.982
2	$(Li_{0.756}Ni_{0.244})_{3a}[Li_{0.157}Ni_{0.843}]_{3b}O_2$	7.125	10.005	3.801
3	$(Li_{0.740}Ni_{0.260})_{3a}NiO_2$	8.227	11.002	4.594

structure was refined with Reitveld method by using the software Rietica for Windows, version 1.7.7. The structure refinement models and their *R* values are given in Table 1. The refinement reveals that the cation distribution in the present sample is $(Li_{0.756}Ni_{0.244})_{3a}[Li_{0.157}Ni_{0.843}]_{3b}O_2$. The refined lattice parameters are $a = 2.8881$ Å, $c = 14.2076$ Å.

The samples for transmission electron microscopy (TEM) observation were prepared following standard preparation procedures, such as polishing, dimpling, and ion-beam thinning. The convergent beam electron diffraction experiments were carried out on a JEM2010–FEF microscope equipped with Omega energy filter, energy dispersive X-ray microanalysis system (EDAX) and Gatan 1024 × 1024 pixels multi-scan CCD camera at the Center for Electron Microscopy of Wuhan University. An energy window of

Table 2
Chemical composition measured by EDAX.

Element	Wt%	At%	*K*-ratio
O	33.60	65.00	0.1297
Ni	66.40	35.00	0.8088
Total	100.00	100.00	

10 eV around the zero-loss energy was elected. Since the energy filter was used in the QCBED experiment, inelastically scattered electrons were not included in the Bloch-wave calculations. The accelerating voltage was 201.5 kV, which was obtained by fitting the dynamically simulated CBED pattern to the experimental pattern taken from a single crystal specimen of silicon.

During QCBED experiments, the chemical composition of the selected grain was measured with EDAX. The result is shown in Table 2. The ratio of Ni at% over O at% equals 35/65, thus the chemical formula is determined as $Li_{0.923}Ni_{1.077}O_2$.

The QCBED experiments were performed under the systematic row diffraction condition. In this condition, the recorded intensities are highly sensitive to the low-order reflections for which the Bragg condition is satisfied. At most, only two or three such structure factors are refined from one energy filtered QCBED pattern. Several QCBED patterns were recorded in different systematic row diffraction orientations.

3. Refinements

3.1. Structure-factor refinements with QCBED method

The refinement is fulfilled by using the program REFINE_CB5 kindly provided by Professor J.M. Zuo at University of Illinois at Urbana-Champaign. With this program the crystal structure factors are refined by fitting the experimental rocking curves to the calculated ones with the Bloch wave method. The absorption coefficients and thickness were also adjusted [14]. The initial value of specimen thickness was roughly calculated by the "two-beam-like" case. The initial amplitudes of structure factors were calculated from independent-atom model, the phase of structure factors are either 0 or π because $LiNiO_2$ is a centrosymmetric crystal.

An example of experimental energy filtered CBED pattern for the (012) systematic row is shown in Fig. 3. In this example, more than 1300 data contained in the three parallel line scans indicated with white lines were used in the refinement. More than 100 structure factors were kept fixed, only 10 of them were refined one by one in the process of refinement. The initial values of U_g and $U_{g'}$ were replaced with the refined values for the subsequent refinements. Finally, the amplitudes of U_g and $U_{g'}$ for the low-order reflections (012) and (024) were refined once more. In each steps, the sample thickness and the start and final points of the line scans were refined simultaneously.

The best fit of the calculated intensity curve to the experimental curve is reached by using the simplex algorithm of optimization. In our experiment, total 11 CBED patterns of six different systematic rows were used in the refinement of the eight structure factors. The results are given in Table 3.

3.2. Multipole refinement

Multipole refinement gives a result which is insensitive to the missing reflections in the X-ray diffraction data, and provides the most efficient parameterization of real space charge density [15]. Multipole refinement was performed with the XD package [13] by

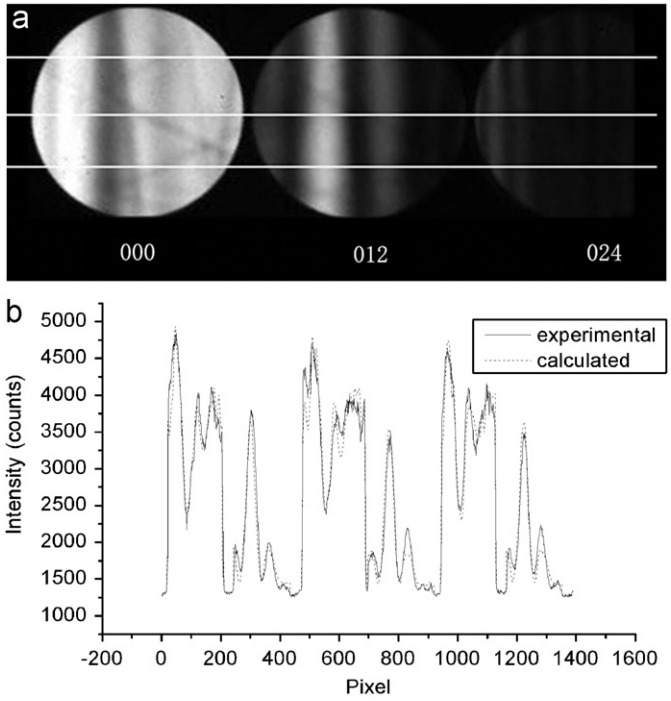

Fig. 3. (a) QCBED pattern of the (012) systematic row diffraction in $LiNiO_2$. (b) Best fit between experiment (solid lines) and theoretically calculated intensities (broken lines) after refinement. For the refinement of the (012) and (024) structure factors, 1392 pixels along three line scans were included.

Table 3
Comparison of the structure factors calculated under kinematical approximation, obtained by X-ray diffraction and obtained by electron diffraction, respectively.

hkl	$\sin\theta/\lambda$ (Å^{-1})	χ^2	F^x_{cal} [a]	$F^x_{X\text{-}ray}$ [b]	F^x_{exp} [c]
003	0.1057	28.86	42.48	45.00	41.62
110	0.3460	24.03	74.30	75.07	77.08
220	0.6921		31.97	33.22	33.14
104	0.2445	45.32	96.11	93.96	97.69
018	0.3454	8.90	73.63	74.87	76.68
012	0.2118	15.34	39.58	42.66	41.01
024	0.4237		60.65	61.05	62.08
101	0.2029	46.31	31.73	32.61	32.46

[a] F^x_{cal} are calculated according to the formula $F^x_g = \sum_j f^x_j \exp\{2\pi i \boldsymbol{g}\cdot\boldsymbol{r}_j\}$, where f^x_j is the atomic scattering factor of j-th isolated atom.
[b] $F^x_{X\text{-}ray}$ are structure factors obtained with single crystal X-ray diffraction. [6]
[c] F^x_{exp} are structure factors obtained firstly with QCBED and then converted to the X-ray structure factors by using the Mott formula.

using eight low-order structure factors measured with electron diffractions as mentioned previously and other 194 structure factors measured with X-ray diffraction [6]. Doing so is based on the following considerations. (1) The results of the Rietveld refinement of X-ray powder diffraction data reveal that the cation distribution is $(Li_{0.756}Ni_{0.244})_{3a}[Li_{0.157}Ni_{0.843}]_{3b}O_2$ which belongs to the same type of cation distribution as that of the single crystal of Ref. [6], and is also very close to $(Li_{0.744}Ni_{0.256})_{3a}[Li_{0.181}Ni_{0.819}]_{3b}O_2$ of Ref. [6]. (2) The chemical composition of the present sample $Li_{0.923}Ni_{1.077}O_2$ is nearly the same as that of the single crystal of Ref. [6], $Li_{0.925}Ni_{1.075}O_2$. (3) The lattice parameters of the present sample are $a = 2.8881$ Å, $c = 14.2076$ Å, which are very close to the data of Ref. [6], $a = 2.8899$ Å, $c = 14.1938$ Å. The ratio $c/a = 4.919$ of the present sample is also close to the value 4.912 of Ref. [6]. The fact that the present ratio of c/a is little bit larger than 4.915 can be considered as being within experimental error. (4) The bonding charge density distribution is mostly determined by the low-order structure factors. However, in measuring the low-order structure factors, the X-ray diffraction is strongly affected by extinction with the error upto 3% which could not be ignored. Hence, the replacement of the low-order structure factors measured by X-ray diffraction with corresponding ones measured by QCBED may improve the determination of the bonding charge distribution.

Table 4
Multipole refinement data.

Refinement parameters	Li	Ni	O
P_{00}	0.0	9.11	6.83
P_{10}			0.063
P_{20}		−0.0308	0.5364
P_{30}			0.081
P_{33}			−0.054
P_{40}		0.0762	0.036
P_{43}		−0.4601	−0.054
κ_{sphv}		1.2550	1.0257
κ_{defv}		0.9167	0.5537
U^{11}	0.026115	0.004919	0.015904
U^{22}	$= U^{11}$	$= U^{11}$	$= U^{11}$
U^{33}	−0.006189	0.004999	0.008859
U^{12}	$= U^{11}/2$	$= U^{11}/2$	$= U^{11}/2$
$R_w(\lvert F\rvert)$ (%)	1.41		

The aspherical atomic electron distribution is divided into three components—core, spherical valence density and deformation electron density [16]. The function is defined as:

$$\rho(\vec{r}) = \rho_c(r) + P_v\rho_v(\kappa r) + \sum_l R_l(\kappa' r)\sum_{m=-l}^{l} P_{lm}Y_{lm}\left(\frac{\vec{r}}{r}\right) \quad (1)$$

The core and spherical valence density are calculated from Hartree–Fock atomic wave function expanded in terms of Slater-type basis functions. In the final term, P_{lm} are the multipole population parameters of each normalized associated Legendre function Y_{lm} of order l, $R_l(\kappa' r)$ is the radial function of the deformation density, also taken as simple Slater functions [17].

Multipoles allowed under the Ni ($\bar{3}m$) and O ($3m$) site symmetries are selected according to the index-picking rules of Kurki-Suonio [18]. In this case, including electron populations in valence orbitals (monopoles), multipoles up to fourth order and corresponding radial expansion (κ) parameters, total 21 additional parameters were refined (see Table 4). The Li atom was treated as spherical ion.

Different scattering tables were tested to refine the combined data set. The calculation using the relativistic Dirac–Fock scattering factors by Su and Coppens [19,20] gives a better fit than using the non-relativistic Hartree–Fock scattering factors by Clementi and Roetti [21].

4. Results and discussion

4.1. Multipole parameters

As seen in Table 4, the larger displacement tensor components U^{ij} for Li atom indicates a strong instability of the Li position in the layered $LiNiO_2$, and unusual small κ_{defv} value of the O atom indicates a larger expand of the O valence shell. As Gougier [22] and Chung [23] reported, there are two different Ni–O bond lengths observed in the $LiNiO_2$ by extended X-ray absorption fine structure (EXAFS) and neutron diffraction, indicating that the

NiO_6 octahedrons are distorted by the Jahn–Teller (JT) effect. However, they also pointed out that this effect is not a long-range but a local JT distortion. So, in view of the whole crystal, the oxygen atom locates averagely around the equilibrium position instead of at a fixed point. The refined coefficient κ_{defv} of oxygen atom shows the extension of the valence shell.

4.2. Electron density and bond critical points analysis

Two maps about the charge density distribution in the Ni–O plane are calculated and plotted. The residual map ($F_{obs}-F_{calc,\ multipole\ model}$) is shown in Fig. 4a. $F_{calc,\ multipole\ model}$ is calculated based on the population parameters refined by the multipole model. Residual map is a measure of the fit of the model to the experimental density distribution, from which the errors may be judged. In this case, the average value of $|\Delta\rho|$ is about 1.0 and $|\Delta\rho|/\rho<0.3\%$, which indicates that a fit with good-quality is obtained. A dynamic model map ($F_{calc,\ multipole\ model}-F_{calc,\ spherical\ atom\ model}$) is shown in Fig. 4b. This map reflects the non-spherical feature around the Ni and the O atoms, and the charge transfer between Ni 3*d* orbital and O 2*p* orbital can be seen. In each Ni–O or Ni–Ni bond, A (3, −1) critical point is found located at each pair of nuclei. The associated properties are derived experimentally and given in Table 5. According to these properties, the Ni–O bond is more like a closed shell interaction, with $|\lambda_1|/\lambda_3$ much less than 1.0, $\rho(r_c)$ less than 1.0 and a positive $\nabla^2\rho(r_c)$ value at the BCP. By BCP properties and by the Fermi-hole function analysis, this is often considered as the bond with some covalent character [24,25]. In the Ni–Ni bond, the BCP properties show the same character, which indicates that there is also a small percentage of covalent character. Similar metal–metal bonding has been reported in Cu_2O and rutile-type compounds [10,26]. The π-bond or σ-bond can be indicated in the bond ellipticity (ε). The ε value of Ni–O bond is very small (<0.05), which supports that the bond which looks like a cylinder has σ-bond character. In contrast, the ε value of Ni–Ni bond is very large, which indicates a π bond character.

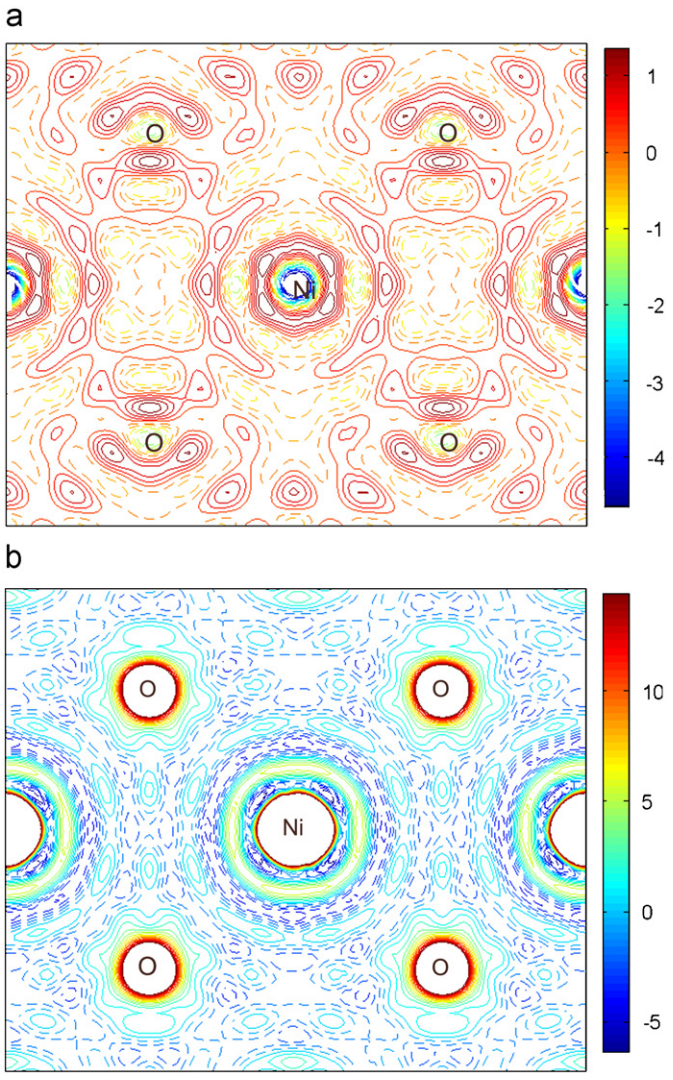

Fig. 4. Charge density distribution on the (841) plane that passes through the central Ni atom and four O atoms within a region of 5.78 Å × 4.82 Å. Solid contours are for $\Delta\rho>0$; dashed contours are for $\Delta\rho<0$. (a) The residual map in which the largest variation is 0.3 eÅ^{-3}. (b) The dynamic model map where the largest variation is 1.0 eÅ^{-3}.

4.3. Ni-atom 3d orbital populations

The refined multipole population parameters enable the calculation of relative *d*-orbital occupancies by using the approach derived by Holladay et al. [27]. In the $LiNiO_2$, the Ni has the site symmetry of $\bar{3}m$. So a 4×4 matrix was used to convert the multipole population to the four canonical *d*-orbital population of a_{1g}, e_g, e'_g and a mixing term $P_4(e_{g+}e'_{g+}+e_{g-}e'_{g-})$. By assuming zero occupancy of the Ni 4*s* and 4*p* orbitals, the individual *d*-orbital occupancies were calculated. The results are listed in Table 6.

As shown in Table 6, the total Ni valence population (monopole) is 9.11e. The electrons preferentially occupy the $e_g(t_{2g})$ and a_g orbitals, and the $e_g(t_{2g})$ orbital has more electrons. The energy level of $e_g(e_g)$ orbital is thought to be higher than those of the $e_g(t_{2g})$ and a_g orbitals. The $e_g(e_g)$ orbital of Ni atom with

Table 6
Ni-atom 3*d* orbital populations calculated from multipole parameters by assuming zero occupancy of 4*s* orbital.

	Spherical atom	Orbital population
a_g	2 (20%)	1.896 (20.82%)
$e_g(t_{2g})$	4 (40%)	4.561 (50.07%)
$e_g(e_g)$	4 (40%)	2.652 (29.12%)
Total 3*d* population (e)	10	9.11

Table 5
Parameters of the bond critical points in $LiNiO_2$.

Bond	BL (Å)	*d* (Å)	$\rho(r_c)$ (eÅ^{-3})	$\nabla^2\rho(r_c)$ (eÅ^{-5})	λ_1 (eÅ^{-5})	λ_2 (eÅ^{-5})	λ_3 (eÅ^{-5})	$\lvert\lambda_1\rvert/\lambda_3$	ε
Ni–O	1.9999	0.959	0.312	9.6	−1.587	−1.563	12.751	0.124	0.015
Ni–Ni	2.8899	1.445	0.12	1.548	−0.464	−0.076	2.087	0.222	5.118

BL is the bond length from experiments. *d* is the distance from BCP to the first atom in the bond. $\varepsilon=|\lambda_1/\lambda_2|-1$ is the bond ellipticity.

their maxima along the metal–ligand bonds loses electrons and the $e_g(t_{2g})$ orbital pointing out of the ligands gains electrons. Like the result that calculated by Iwata in $[Co(CN)_6]^{3-}$ [28,29], in the similar low-spin complexes the population of $e_g(e_g)$ orbital is depopulated relative to the spherical atom, but the remaining non-zero population of $e_g(e_g)$ indicates that there are covalent bonding features between the metal Ni and ligand O.

5. Conclusions

Low-order electron structure factors of $LiNiO_2$ were refined accurately by QCBED method. Combining these structure factors with X-ray measurements in a multipole refinement, the multipole analysis data, detailed properties at BCP and the 3*d* orbital populations of Ni atoms were obtained. Based on these results, it is found that the bonding between the metal and oxygen atoms has σ bond character with covalent feature, and the bonding between two metal atoms has π bond character also with some covalent component. By assuming zero 4*s* population, the total number of *d*-electrons is then determined as 9.11 for Ni from the present experiments, and the population of a_g, $e_g(e_g)$ and $e_g(t_{2g})$ orbital are also obtained.

Acknowledgments

We are very grateful to Dr. J. Akimoto for providing the X-ray diffraction data of single crystal $LiNiO_2$. We also want to thank Professor J.M. Zuo for providing the source code of his program REFINE_CB5 for structure factor refinement of crystals. This work was supported financially by the National Natural Science Foundation of China (no. 50671073).

References

[1] J.B. Goodenough, D.G. Wickham, W.J. Croft, J. Phys. Chem. Solids 5 (1958) 107.
[2] M.G.S.R. Thomas, W.I.F. David, J.B. Goodenough, P. Groves, Mater. Res. Bull. 20 (1985) 1137.
[3] V. Bianchi, D. Caurant, N. Baffier, C. Belhomme, E. Chappel, G. Chouteau, S. Bach, J.P. Pereira-Ramos, A. Sulpice, P. Wilmann, Solid State Ionics 1 (2001) 140.
[4] J. Molenda, P. Wilk, J. Marzec, Solid State Ionics 73 (2002) 146.
[5] A. Rougier, P. Gravereau, C. Delmas, J. Electrochem. Soc. 143 (1996) 1168.
[6] Y. Takahashi, J. Akimoto, Y. Gotoh, K. Kawaguchi, S. Mizuta, J. Solid State Chem. 160 (2001) 178.
[7] S.L. Dudarev, L.M. Peng, S.Y. Savrasov, J.M. Zuo, Phys. Rev. B 61 (2000) 2506.
[8] F. Reynaud, D. Mertz, F. Celestini, J.M. Debierre, A.M. Ghorayeb, P. Simon, A. Stepanov, J. Voiron, C. Delmas, Phys. Rev. Lett. 86 (2001) 3638.
[9] A.J.W. Reitsma, L.F. Feiner, A.M. Oles, New Journal of Physics 7 (2005) 121.
[10] J.M. Zuo, M. Kim, M. O'Keeffe, J.C.H. Spence, Nature 401 (1999) 49.
[11] B. Jiang, J.M. Zuo, N. Jiang, M. O'keeffe, J.C.H. Spence, Acta Cryst. A 59 (2003) 341.
[12] J. Friis, B. Jiang, J. Spence, K. Marthinsen, R. Holmestad, Acta Crys. A 60 (2004) 402.
[13] T. Koritsanszky, P.R. Mallinson, S. Howard, A. Volkov, P. Macchi, Z. Su, C. Gatti, T. Richter, L.J. Farrugia, N.K. Hansen, XD-A computer program package for multipole refinement and analysis of electron densities from diffraction data, Version 4.11, State University of New York at Buffalo, 2004.
[14] J.M. Zuo, J.C.H. Spence, Ultramicroscopy 35 (1991) 185.
[15] R. Restori, D. Schwarzenbach, Acta Cryst. B 42 (1986) 201.
[16] N.K. Hansen, P. Coppens, Acta Cryst. A 34 (1978) 909.
[17] E. Clementi, D.L. Raimondi, J. Chem. Phys. 38 (1963) 2686.
[18] K. Kurki-Suonio, Isr. J. Chem. 16 (1977) 115–123.
[19] Z. Su, P. Coppens, Acta Cryst. A 54 (1998) 646.
[20] P. Macchi, P. Coppens, Acta Cryst. A 57 (2001) 656.
[21] E. Clementi, C. Roetti, At. Data Nucl. Data Tables 14 (1974) 177.
[22] A. Rougier, C. Delmas, A.V. Chadwick, Solid State Commun. 94 (1995) 123.
[23] J.H. Chung, Th. Proffen, S. Shamoto, A.M. Ghorayeb, L. Croguennec, W. Tian, T. Egami, Phys. Rev. B 71 (2005) 064410.
[24] T. Song, H. Wang, Y. Wang, J. Phys. Chem. A 102 (1998) 3726.
[25] C.R. Lee, C.C. Wang, K.C. Chen, G.H. Lee, Y. Wang, J. Phys. Chem. A 103 (1999) 156.
[26] P.I. Sorantin, K. Schwarz, Inorg. Chem. 31 (1992) 567.
[27] A. Holladay, P. Leung, P. Coppens, Acta Cryst. A 39 (1983) 377.
[28] M. Iwata, Y. Saito, Acta Cryst. B 29 (1973) 822.
[29] M. Iwata, Acta Cryst. B 33 (1977) 59.